Identification and Characterization of a Buried Volcanic Field Using Seismic Reflection and Borehole Data

Alan Bischoff [a]*, Marcos Rossetti, Andrew Nicol and Ben Kennedy

[a] *Department of Geological Sciences, University of Canterbury, Christchurch, New Zealand;*

alan.bischoff@canterbury.ac.nz *corresponding author\

This is a non-peer reviewed preprint submitted to EarthArXiv.

It has been submitted on February 13, 2019 to Bulletin of Volcanology.

Abstract

Buried volcanoes occur in great numbers within sedimentary basins globally. Knowledge of ancient buried volcanic systems has improved significantly over the past two decades. The in-depth understanding of these buried systems was mainly possible due to increasing availability of high-quality seismic reflection and sub-surface borehole data. This paper examines a cluster of Miocene volcanoes now buried by ca 1000 m of sedimentary strata in the Canterbury Basin, New Zealand. These volcanoes were imaged by 2D seismic lines and perforated by the Resolution-1 borehole. We refer to this group of volcanoes and related intrusive bodies as the Maahunui Volcanic Field (MVF). Here, we present detailed petrographic and seismic reflection interpretation of some representative volcanoes of the MVF, and of the strata that enclose them, to constrain the environments in which intrusions and eruptions occurred. Intrusive rocks penetrated by the Resolution-1 comprise a monzogabbro body with a saucer-shape geometry emplaced in organic-rich sedimentary layers. The monzogabbro contains miarolitic cavities and ophitic textures which, together with decompaction of its overburdened sedimentary strata, suggest an emplacement depth around 950 m below the paleo-seafloor. Seismic lines show an array of faults at the tips of the saucer-shaped monzogabbro. These faults are connected with the root of some volcanoes, and may have formed feeder systems for eruptions and hydrothermal fluids onto the Miocene paleo-seafloor. Volcaniclastic rocks comprise abundant glassy shards, relics of bubble walls, spheroidal fragments enveloped in a palagonite film, broken phenocrysts, and lithics. These volcaniclastic rocks are interbedded with lower bathyal siltstones, indicating that eruptions near the location of the Resolution-1 occurred in a deep-submarine environment (1000-1500 m). Integration of petrographic, geochemical and seismic reflection interpretations suggest that the volcaniclastic rocks have a genetic relationship with the saucer-shaped monzogabbro, which may have served as a shallow stationary magma chamber for some volcanoes in the MVF. The available data indicate processes of intense material fragmentation and particle dispersion, consistent with phreatomagmatic eruptions, although globally this eruptive style is rarely interpreted to occur at water depths around 1000 m. The emplacement of intrusions into organic-rich sedimentary rocks could incorporate thermogenic gases into the magmatic system, providing supplementary driving forces to form large deep-water pyroclastic eruptions.

Keywords: buried volcanoes; seismic reflection; deep-water eruptions.

Introduction

Buried volcanoes are common in sedimentary basins globally (e.g. Field et al. 1989; Holford et al. 2012; Giba et al. 2013; Planke et al. 2017). These “fossil” volcanoes are the remains of ancient volcanic systems that erupted onto the Earth’s surface in the past, which are now buried and preserved within sedimentary strata in the subsurface. Advances in seismic interpretation techniques together with an increasing availability of high-quality seismic data have helped to significantly improve our understanding of volcanoes preserved in sedimentary basins. Characterization of buried volcanoes is often best achieved by integrating large datasets of 2D and 3D seismic surveys, along with biostratigraphic, geochronological, geochemical, petrophysical and petrographic information from boreholes (e.g. Planke et al. 1999; Single and Jerram 2004; Schofield et al. 2016; McLean et al. 2017). Interpretation of these datasets as part of a multidisciplinary approach that correlates insights from disciplines such as stratigraphy, sedimentology and volcanology can produce unified models to explain the genesis and evolution of buried volcanic systems (e.g. Herzer 1995; Planke et al. 2000; Bischoff 2019). Information from these complementary datasets provide improved knowledge of the main geological processes that create, transform, and preserve volcanoes now buried in sedimentary basins (e.g. Huafeng et al. 2015; Reynolds et al. 2016; Bischoff et al. 2017; Infante-Paez and Marfurt 2017).

The present work studies part of a cluster of middle Miocene volcanoes currently buried by ca 1000 m of sedimentary strata in the offshore Canterbury Basin, east of New Zealand's South Island (Figure 1). We refer to these volcanoes as the Maahunui Volcanic Field (MVF), from the Māori name for the stretch of coast south of Banks Peninsula (aka Canterbury Bight) and immediately adjacent to the study area. Volcanic activity of Miocene age was previously identified in the study area by 2D seismic reflection surveys, and by intrusive and extrusive rocks sampled in the Resolution-1 petroleum exploration well (Milne 1975; Field et al. 1989). Despite an initial effort to recognize these buried volcanoes, important information on their origin and evolution was missing prior to the present study.

The geological history of the MVF is presented in three inter-related papers, although each one can be read and understood separately. This is the first paper and focuses on seismic reflection analysis in the vicinity of the well Resolution-1, and on the petrographic characterization of the igneous rocks and enclosing sedimentary strata sampled in this well. The second paper (Bischoff et al. 2019a) is designed to present the results of the seismic morphological and paleogeographic reconstruction of the MVF area, in which we up-scale interpretations from the location of the Resolution-1 to a regional scale. In the third paper (Bischoff et al. 2019b), we unravel the complete architecture of the MVF from emplacement to burial, characterizing its main intrusive, eruptive, and sedimentary architectural elements, and their impact on geoenergy resources such as hydrocarbons and geothermal energy. The knowledge of the "fossil" volcanoes of MVF can provide useful insights of how volcanic fields form and evolve elsewhere, including their perceived geological hazards, and potential to contain socio-economical resources.

Geological Setting

Sedimentation in the northern Canterbury Basin began in the late Cretaceous, after the initial stages of the separation of Zealandia from eastern Gondwana and opening of the Tasman Sea. In the study area, paralic to shallow marine conditions prevail until the early Eocene, with deposition of sandstones, mudstones and coal beds of the Broken River and Conway Formation, and Charteris Bay Sandstone. Continuous marine transgression throughout the late Paleogene favour the formation of shallow-to deep-water sediments of the Ashley Mudstone and Amuri Limestone. In the early Neogene, the present oblique-convergent boundary between the Pacific and Australian plates induced uplift and erosion of the western part of the Canterbury Basin, with progradation of marine to continental sediments of the Tokama and Kowai Formation towards the southeast (e.g. Suggate et al. 1978; Field et al. 1989; Kamp et al. 1992; Mortimer et al. 2004; Strogen et al. 2017; Barrier 2019; Figure 2 and 3).

Igneous rocks often pierce and interbed with strata of the northern Canterbury Basin sedimentary succession. Onshore, the most expressive products of volcanism is represented by the Mount Sommers Volcanic Group (Cretaceous), View Hill Volcanics (Eocene), and Miocene igneous rocks of the Burnt Hills Group and Banks Peninsula (e.g. Carlson et al. 1980; Field et al. 1989; Forsyth et al. 2008; Figure 1 and 3). The offshore Canterbury Basin contains several late Cretaceous to Pleistocene buried volcanoes and intrusive igneous bodies identified by seismic reflection mapping and borehole data (e.g. Field et al. 1989; Blanke 2010; Bischoff et al. 2016; Barrier et al. 2017). Middle Miocene igneous rocks were first identified in the study area by the petroleum exploratory Resolution-1 well, drilled in 1975 (Figure 1, 2 and 3). This borehole penetrated volcaniclastic rocks interbedded with deep-water siltstones of Waiauan age (12.7 to 11 Ma) from 1103.5 to 1220 m and intersected a coarse-grained intrusive body at 1911 m, which was K-Ar dated at 12 ± 2 Ma (Milne 1975).

Successive authors tentatively correlated the igneous rocks of Resolution-1 with outcrops of volcanic rocks on the Banks Peninsula, the Acheron Outlier intrusions (Milne 1975), and Harper Hills Basalt (Field et al. 1989; Figure 1). Banks Peninsula is a large polygenetic composite-shield volcanic complex mainly erupted subaerially during the late Miocene (Sewell 1988). Harper Hills Basalt comprises a sequence of subaerial tholeiitic lava flows K-Ar dated at 10.5 ± 0.3 Ma (Carlson et al. 1980; Browne 1983), and associated volcanic muds (Coalgate Bentonites), basaltic dikes (Bluff Basalt), and well-bedded volcaniclastic rocks (Sandpit Tuff). Biostratigraphic dating suggests that the Sandpit Tuff dates either from Waiauan (12.7 to 11 Ma) or Tongaporutuan (11 to 7.2 Ma), according to Carlson et al. (1980) and Browne (1983). Acheron Outlier intrusions are tholeiitic gabbros forming a large irregular laccolith emplaced along Cretaceous to Paleocene paralic rocks of the Eyre Group, and were most likely formed in the Oligocene (Eady 1995). Carlson et al. (1980) identified early-to-middle Miocene tuffaceous rocks interbedded with shallow marine to estuarine sedimentary strata outcropping near Coalgate (Wairiri Volcaniclastite; Figure 1). These volcaniclastites comprise volcanic silts, sands, and tuff-breccias that contain basaltic lava fragments, glass, and abundant palagonite. Petrographically, Wairiri Volcaniclastite is the closest outcropping correlative of the volcaniclastic rocks penetrated by Resolution-1, however these volcaniclastites were erupted in a shallow-water environment, while volcaniclastics of the MVF were erupted in a deep-water.

Dataset, Methods and Limitations

We use more than 40,000 km of high-quality 2D seismic lines in correlation with data from six drilling wells (Leeston-1, Clipper-1, Ealing-1, Resolution-1; Charteris Bay-1 and 2). Ten regional chronostratigraphic surfaces from the early Miocene to the modern seabed were mapped in detail using 2D seismic lines. (Figure 1 and 2). Before mapping, the seismic reflection lines from the New Zealand Petroleum and Minerals (NZPAM) Kingdom© project were checked and calibrated with check-shot surveys from the Resolution-1 and Clipper-1 wells (Milne, 1975 and Hawkes and Mound 1984). The depths of chronostratigraphic markers and formation tops were verified and, where necessary, corrected using the revised biostratigraphy of the Canterbury Basin published by Schiøler et al. (2011). Subsequently, we mapped two important early Miocene (eM) and late Miocene (lM) unconformities, based on the stratal relationship of seismic reflectors including types of terminations and depositional trends (Catuneanu 2006), and following criteria from “sequence boundary” defined by Hunt and Tucker (1992). In addition, we have undertaken a seismic volcano-stratigraphic analysis (Planke et al. 1999) for the study area by mapping the lateral continuity of the pre- and post-eruptive surfaces (PrErS, PoErS) of the MVF (Figure 4).

This mapping correlates the first and last occurrence of middle Miocene extrusive rocks in the Resolution-1 well with seismic anomalies that could represent buried volcanoes of the same age.

We described and photographed relevant rock intervals of the Resolution-1 at the New Zealand Petroleum and Minerals core-store. One drill-core of an intrusive rock from a depth of 1962.25 m and thirteen composite cutting samples of volcaniclastic rocks at 10 m intervals between 1100 to 1230 m depth were used here to perform macro-and-microscopic petrographic analysis. Petrographic characterization of these cuttings samples may have limitations due to factors including, small original grain size, potential break-up of material during drilling operations, composite sample intervals that likely blend material from diverse beds, and the difficulty of separating drilling mud from altered *in situ* volcanic fragments. Due to the high degree of alteration of some of the cuttings samples, conventional sample washing to separate drilling mud from sampled material was not applied because most of the soft rock material would have been lost during the sieving process. Therefore, to prepare the samples we have adopted a dry-and-wet manual “grain-by-grain” separation of potential volcanic fragments from drilling mud.

X-ray fluorescence (XRF), Scanning Electron Microscope (SEM) and Energy Dispersive Spectroscopy (EDS) analysis were performed on samples from selected intervals containing igneous rocks. Qualitative XRF was conducted using an Olympus Vanta handheld analyzer for one sample from 1962.25 m depth (intrusion) and three samples from 1130 to 1160 m depth (volcaniclastics). The handheld XRF machine was calibrated to perform a bulk geochemistry analysis of the total sample. Although this handheld cannot detect Na, it can detect other essential (Si, Ca, K, Ti, Mg) and incompatible elements (Zr, Y, Ti, Nb). Thus, we compare the chemical composition of the MVF intrusive and extrusive rocks using the Zr/Ti versus Nb/Y diagram proposed by Pearce (1996) after Winchester and Floyd (1977). SEM and EDS analysis were performed at the Electron Microscopy Centre at the University of Canterbury, with the aim of characterizing the elementary chemical composition of fragments collected from a depth range of 1140 to 1150 m (volcaniclastics), and to detail the morphology of the volcaniclastic fragments.

Characterization of the Igneous Rocks and Enclosing Sedimentary Strata of the MVF

The Resolution-1 borehole penetrates five main groups of rocks that comprise and enclose the MVF. These are (from deepest to shallowest): (I) intrusive rocks emplaced into (II) host paralic to neritic sedimentary rocks, (III) bathyal mudstones and limestones, and (IV) bathyal siltstones interbedded with (V) volcaniclastic rocks.

Rock Association I: Intrusive rocks (1963 to 1911.5 m)

Resolution-1 penetrates 51.5 m of intrusive rocks from 1963 to 1911.5 m, approximately 5 m of which was cored from 1963 to 1958 m. Petrographic description of a core sample collected from a depth of 1962.25 m indicated a medium-grained, hypidiomorphic olivine monzogabbro with ophitic and sub-ophitic textures (Figure 5). The major mineral phases in this core sample are plagioclase (70%), which forms elongated euhedral to subhedral crystals (0.5 to 2.5 mm), and clinopyroxene (20%) that occurs as subhedral prismatic crystals (up to 6 mm). Prismatic subhedral orthoclase (1 - 2 mm) and crystals of olivine (1 mm) occur in small amounts (<5%), accompanied by minor apatite and ilmenite (<3%). Plagioclase crystals can be partially or totally enclosed in prismatic crystals of clinopyroxene (ophitic and sub-ophitic texture), suggesting that the plagioclase started to crystalize before clinopyroxene. These mineral phases and textures are typical of diabase rocks and suggest an intermediate magma cooling rate at shallow depths (Walker 1957).

In some parts of the sample, the monzogabbro is altered to chlorite (Figure 5a, d and g), which is interpreted to record effects of hydrothermal alteration at relatively high temperature (ca 250° C). The plagioclase (from andesine to labradorite composition based on their extinction angle) is commonly altered to smectite, illite, sericite and zeolite. The clinopyroxenes (augite) in some cases are replaced by amphibole and biotite (Figure 5d). Subhedral olivine grains are in general fractured and partially replaced by iddingsite, which indicates oxidizing conditions (Smith et al. 1987).

The petrographic description presented in Milne (1975) classified some parts of this intrusion as a quartz-monzogabbro, and as a teschenite, due to the presence of analcite. However, quartz crystals were absent in our samples, and we only identified rare crystals of analcite associated with radial zeolite (Figure 5a, f and i), which always occurs filling residual space and cavities. This suggests that analcite is more likely a secondary product of hydrothermal alteration rather than a primary mineral that originates from the melt. Miarolitic cavities were described in several parts of the core (Figure 5f) reinforcing the petrographic interpretations of a hypabyssal rock injected at shallow depths, and may indicate that MVF melts were enriched in volatiles (Peretyazhko 2010).

Rock Association II: Paralic to neritic host sedimentary rocks (1911 to 1335 m)

The monzogabbro intrusion (Rock Association I) was emplaced into Cretaceous-Paleocene paralic to neritic sedimentary rocks of the Broken River and Conway formations (Rock Association II). These sedimentary rocks comprise granular pebble-sized conglomerates, fine-grained white quartz sandstones, dark grey pyritic siltstones, and thin layers of carbonaceous mudstones. Abundant carbonate and zeolite veins indicate that hydrothermal activity extended at least 34 m above the intrusion (Milne 1975). Palynomorphs and miospores show an increasing degree of thermal alteration towards the intrusion (Schiøler et al. 2011). Onshore, similar gabbroid rocks (Acheron Outlier; for location see Figure 1) show thermal effects extending several tens of meters from the igneous rocks (Eady 1995). Intrusions emplaced in organic-rich sedimentary rocks have the potential to elevate the temperature near the igneous bodies sufficiently high to generate thermogenic gas (Aarnes et al. 2015). Heating of organic material can generate methane (CH_4), and release high amounts of greenhouse gases such as CO_2 (Delmelle et al. 2015; Svensen et al. 2018) and H_2S (e.g. Iacono-Marziano et al. 2013; Robertson et al. 2015; Arnorsson et al. 2015).

The upper Paleocene-Eocene part of Rock Association II is characterized by mudstones and fine-grained sandstones (Charteris Bay Sandstone), interpreted to have been deposited in a transgressive shallow-marine environment during passive subsidence of the basin (Field et al. 1989; Schiøler et al. 2011). Rock Association II is locally interbedded with thin layers of tuffaceous rocks that likely correspond to material erupted from scattered vents in the Canterbury Basin.

Rock Association III: Bathyal mudstones and limestones (1335 to 1284 m)

The light grey to brown mudstones (Ashley Mudstone) and light grey massive limestones (Amuri Limestone and Omihi formations) of Rock Association III were deposited during the Oligocene to early Miocene. These rocks are typically poorly indurated and comprise silty mudstones to calcareous mudstones and wackestones separated by gradational boundaries (Milne 1975; Figure 6). They also contain rare tuffaceous material that likely erupted from scattered vents in the Canterbury Basin. Rock Association III represents the time interval of maximum inundation of Zealandia, and in the study area, corresponds to the development of a condensed section attributed to a low supply of terrigenous material (Field et al. 1989). The contact between the Amuri and Omihi formations in the Resolution-1 well is unconformable, with a time break of ca 13.5 million years, from the early Oligocene to early Miocene in the study area (unconformity O-eM; Figure 3 and 6). The origin of the O-eM unconformity is controversial and successive authors have interpreted it to be the product of glacio- or tectonic-eustatic changes, sediment starvation during a high stand period, volcanism, or action of sea-bottom currents (Lever 2007).

Rock Association IV: Bathyal siltstones (1284.1 to 686.1 m)

Rock Association IV comprises a soft light grey siltstone (Tokama Siltstone) with sparse bioclasts and foraminifera fossils (Figure 7a). These rocks were deposited in a bathyal setting from the early Miocene to early Pliocene (Milne 1975; Schiøler et al. 2011). Rock Association IV is locally interbedded and blended with volcaniclastic material of the MVF (rocks association V; Figure 7b, c and d). Three main unconformities are identified by biostratigraphic data in this siltstone at the Resolution-1 well, each representing hiatuses of 1 to 3 Ma (Schiøler et al. 2011). These unconformities are interpreted to have formed by different tectonic pulses during the onset of basin inversion and contractional tectonics NW in the study area, which is related to southward propagation of the Neogene Hikurangi subduction zone (e.g. Field et al. 1989; Kamp et al. 1992; Lu et al. 2005; Schiøler et al. 2011). Here, we refer to these unconformities as eM (early Miocene), lM (late Miocene), and eP (early Pliocene), according to their ages (Figure 3 and 6).

To characterize in detail the paleoenvironment in which the MVF has erupted, we subdivide the Tokama Siltstone into four depositional units. These units are bounded by unconformities or correlative marine conformities, recording major paleo-bathymetric changes identified in the biostratigraphic data of Resolution-1 (Schiøler et al. 2011). Table 1; Figure 3 and 6 show the main stratigraphic and paleo-environment characteristics of these units.

The lower Tokama was deposited during the late-early Miocene in a deep-to-lower bathyal setting, with water depths ranging from 2000 to 1500 m (Figure 6). Its upper boundary is marked by a sharp transition to a lower bathyal setting (1500 to 1000 m), which coincides with the unconformity eM, locally representing a ca 1.5 Ma hiatus in sedimentation (Figure 6).

The middle Tokama was deposited during the middle Miocene, simultaneous with volcanic activity in the MVF. This rock association formed in a relatively steady lower bathyal setting (1500 to 1000 m deep), evident by the biomarker species *Sigmoilopsis schlumbergeri* and *Eggerella bradyi*, often associated with *Cibicides robertsonianu*. Up the well, the decreasing content of planktic species indicates an overall decrease in water depths during the late-middle Miocene (Schiøler et al. 2011; Figure 6). We place the onset of this base-level fall at ca 11 Ma, based on seismic stratigraphic analysis that shows a NW-SE progradation of self-slope clinoforms, which produces decreasing water depths in the study area (Figure 4).

The onset of decreasing water depths at ca 11 Ma marks the base of the upper Tokama, which is interpreted to represent a progressive shift from a lower bathyal to a middle bathyal setting (800-600 m). Seismic stratigraphy mapping demonstrates that before 11 Ma, the volcanoes of the MVF were extinct (Bischoff et al. 2019b). The top of the upper Tokama is marked by a sharp transition to an uppermost bathyal setting (400-200 m) and associated hiatus of ca 1 Ma in the study area (unconformity lM).

The uppermost Tokama (Figure 6) was deposited during the late Miocene to early Pliocene in an uppermost bathyal setting. Seismic stratigraphic interpretation suggests a progressive shallowing in water depths up-sequence. The top of this depositional unit is marked by the occurrence of bioclastic mudstones, coquinas and sandstones of the Kowai Formation starting at 686.1 m. Sediments of the Kowai Formation mark the establishment of an outer neritic setting (100 to 200 m) in the area of the well, which occurred around 5.3 Ma (unconformity eP, Figure 3).

Rock Association V: Volcaniclastic rocks (1220 to 1103.5 m)

Rock Association V comprises poorly sorted, hyalocrystalline, altered and non-welded fragments of leucocratic rocks, with frequent glassy shards and broken crystals interbedded with the bathyal siltstones of Rock Association IV (Figures 7 to 12; Table 1). Grain-size distribution is variable (< 0.1 to 5 mm), usually comprising fragments with microcrystalline, microporphyritic, vitrophyric, and less frequently, vitriclastic textures (Figure 8). Primary components include crystals of plagioclase and pyroxene, shards of glass (Figure 9 and 10), and spherical aggregates of microcrystals and devitrified glass. Sandstone, coal and limestone lithics are abundant (Figure 7 and 11c and f), showing petrographic similarities with those of Rock Associations II and III. Pervasive palagonite alteration is dominant, although some fresh glass is also observed.

Elongated euhedral crystals of plagioclase are usually <0.1 to 1.5 mm in size, and are typically associated with microporphyritic and vitrophyric textures (Figure 8). Plagioclase often occurs as euhedral to anhedral broken phenocrysts in sharp contact with the groundmass (Figure 8b, c and f). Some phenocrysts show rounded margins, (Figure 8d) and some rare phenocrysts show sieve texture and devitrified glass inclusions (Figure 8e).

Glassy shards are dominant and occur in a wide range of shapes and textures. Commonly, shards are non-welded and present blocky and cuneiform shapes, and less frequently, cuspate, platy and splintery shapes, and relics of bubble walls (Figure 9 and

10). In some samples, these spall shards show jigsaw-fit texture, typically together with blocky fragments containing a microporphyritic core (Figure 9). Very-fine anhedral broken crystals often occur in association with shards showing cuspate, platy and pumice shapes, typically together with pervasive alteration to palagonite (Figure 10).

The spherical aggregates of microcrystals and devitrified glass show two styles: (i) poorly-indurated spherules with or without an inner core (possible a lithic fragment), usually enveloped in a palagonite film (Figure 11a, d and e), and (ii) well-indurated spherules that contain a devitrified (palagonite) inner core, a single concentric outer rim, and an external array of acicular crystals in a radial pattern, typically associated with perlitic cracks (Figure 12). In both styles, the spherical aggregates occur in association with rocks showing a pervasive palagonite alteration.

Geochemistry of representative igneous rocks of MVF

The dominant mineral paragenesis comprising plagioclase, pyroxene and olivine of both intrusive and extrusive rocks indicate that the volcanoes in the MVF, at least partially, were sourced from primitive basaltic melts. XRF results for both monzogabbro and volcaniclastic rocks indicates proportional content of SiO_2, Al_2O_3, MgO, Fe_2O_3, CaO, K_2O_5, P_2O_5, TiO_2 and MnO (Appendix 1). The ratio of incompatible elements of both rock types, when plotted in a Zr/Ti versus Nb/Y diagram (Pearce 1996; after Winchester and Floyd 1977), suggests a basaltic alkaline magmatic series (Figure 13). The dominant palagonite alteration, which is typically interpreted as the product of devitrification of sideromelane glass (Stroncik and Schmincke 2002), also indicates an original basaltic composition. In addition, EDS analysis of volcanic glass fragments reinforced a basaltic composition for the MVF melts (Appendix 2).

The similar compositional signature of all MVF igneous rocks can be interpreted to indicate a genetic correlation between the monzogabbro intrusion and the middle

Miocene volcaniclastic fragments. The close chemical relationship between intrusive and extrusive volcanic rocks is consistent with data from seismic reflection lines in the location of the well, which collectively suggest that these rocks formed in close spatial and temporal association (Figure 14 and 15). It is important to recognize that the geochemical analysis presented here was performed only to verify a possible compositional correlation between the intrusive and extrusive rocks. Further detailed geochemical studies are required to characterize the magmatic evolution of the MVF.

Age and Formation of the MVF

To estimate the age of active volcanism in the MVF, we consider biostratigraphic data (Schiøler et al. 2011), a K-Ar date of the monzogabbro intrusion (Milne 1975), sedimentological aspects of the strata that enclose both intrusive and volcaniclastic rocks (i.e. amount of compaction and sedimentation rates), and results from seismic stratigraphic mapping (Figure 6, 14 and 15). The oldest MVF volcaniclastic rocks (1220 m in the well) coincide with the boundary between the Lillburnian and the lower Waiauan New Zealand stages (ca 12.7 Ma), thus, we assume an onset of volcanism in MVF at 12.7 Ma (Figure 3 and 6). The youngest volcaniclastics occur at 1103.5 m in the well, however, there is no direct biostratigraphic age correlation at this depth (Figure 6). To define the cessation of volcanic activity in the MVF, we calculated the sedimentation rates of the middle and upper Tokama, for the depth interval between 1255 and 1030 m in the well (Figure 6). The difference in thickness and age of this interval are 215 m and 2.59 Ma, respectively. To reduce the effect of the thickness of volcanic rocks on sedimentation rates, we subtract 10 m, which was estimated from the density and gamma logs in the well (Figure 6). This gives an average sedimentation rate of 83 m/Myr. Assuming that the sedimentation rate was constant at Resolution-1 during the formation of the MVF, siltstone thickness of 106.5 m for the MVF interval would have been deposited over ca 1.2 Ma (i.e. 106.5 m / 83 Myr/m). Thus, MVF volcanism started at ca 12.7 Ma and may have ceased at about 11.5 Ma, which is consistent with the K-Ar age of crystallization of the intrusion (12 ± 2 Ma; Milne 1975).

To estimate the depth of the saucer-shaped monzogabbro emplacement, we first subtract the depth of the surface marking the onset of volcanism in the MVF (1220 m in the well), from the depth of the top of the intrusion in the well (1911.5 m), which produces a difference of 691.5 m. Next, we assume uniform compaction for the overlying sedimentary pile of 40%, using compaction curves for sediments in the Canterbury Basin presented in Field et al. (1989). These calculations give us an emplacement depth of ca 950 m below the contemporary middle Miocene paleo sea-bed, which is consistent with the shallow level monzogabbro intrusion with ophitic texture and miarolitic cavities. Results from the decompaction and backstripping of the sedimentary overburden above the saucer-shaped monzogabbro presented in Magee et al. (2019), suggest an emplacement depth of ca 800 m beneath the contemporaneous middle Miocene surface, which is consistent with our results.

The age relationship of the monzogabbro and volcaniclastic rocks is reinforced by seismic lines that show sedimentary strata force-folded into a dome shape above the intrusive body. Middle Miocene sediments, including the volcaniclastics of the MVF, onlap the uppermost termination of these folds. The doming consequentially changed the Waiauan paleo-sea floor topography and promoted deposition as channelized systems of latest Waiauan age (11.5 to 11 Ma) next to the dome structures (Figure 14). Seismic lines that image the saucer-shaped monzogabbro show disrupted reflectors and faults at the tips of this intrusive body, possibly representing pathways for magma and hydrothermal fluid migration up-sequence (Figure 15). In some cases, these faults are connected with the root of volcanoes, indicating a possible feeding system for eruptions onto the middle Miocene paleo-sea bed. Integration of results from petrography, geochemistry and seismic interpretation suggests that the volcaniclastic rocks were at least partially erupted by magmas sourced from the saucer-shaped monzogabbro. This shallow intrusion has likely acted as a stationary magma chamber for some of the volcanoes of the MVF.

Discussion

The volcanic textures recognized in this study confirm a volcanogenic origin of the seismic anomalies previously interpreted to correspond to volcanoes buried in the Canterbury Basin (Field et al. 1989). However, these textures could not provide all of the necessary information to interpret past-eruptive styles of the volcanoes in MVF. For example, broken phenocrysts of plagioclase with sharp edges (Figure 8) could represent fragments of holocrystalline material crystalized in the magma chamber that was disaggregated by pyroclastic or autoclastic processes when erupted at the surface (McPhie et al 1993; Best and Christiansen 1997). The presence of phenocrysts with rounded margins (Figure 8d) may be caused by abrasion due to particle collision during magmatic transport, or mixing and recycling of material associated with multiple explosions into deep crater zones of maar-diatreme volcanoes (White and Ross, 2011; Graettinger et al. 2016). Shards with blocky, cuspate, platy, relics of bubble walls and pumice shapes, together with very fine-grained rocks with a pervasive alteration to palagonite (Figure 10) may indicate mechanisms of intense fragmentation such as those experienced in phreatomagmatic eruptions (e.g. Walker and Croasdale 1971; McPhie et al. 1993). However, White and Valentine (2016) argue that the particle morphology and fragment size may not contain all the necessary information to diagnose the products of magmatic versus phreatomagmatic eruptions. These spall shards with jigsaw-fit texture, in association with blocky fragments with microporphyritic cores could represent fragments of hyaloclastites or could be formed at the chilled crust of submarine spatter-like deposits (Cas and Giordano 2014; Cas and Simmons 2018). The spherical-shaped fragments (Figure 11 and 12) may represent both armoured lapilli formed as a product of eruption-fed density currents (White 2000; Agirrezabala et al. 2017), and/or spherulites, which are commonly interpreted to indicate high-temperature devitrification of coherent volcanic glass (Marshall 1961; Lofgren 1970; apud McPhie et al. 1993).

Combining petrographic and seismic reflection interpretations constrains the eruptive styles in the MVF. Near the location of Resolution-1, seismic imagery shows deep craters excavated into the PrErS horizon (Figure 4 and Figure 15). The roots of these craters terminate at the depth of the underlying Eocene-Oligocene limestone and sandstone units, which likely provide the common lithic fragments found in the MVF volcaniclastic rocks (Figure 11). Deep excavations into the PrErS requires significant energy and intense material fragmentation (e.g. Lorenz 1985; Zimanowski et al. 1997; Kereszturi and Németh 2013; White and Valentine 2016), which together with the textures of the volcaniclastic rocks may be strong evidence of phreatomagmatic activity in the MVF. The presence of frequent lithics of coal (Figure 7), possibly from the underlying Cretaceous Broken River Formation, may indicate that thermogenic gases (CH_4) or CO_2 could be incorporated into the magmatic system. The addition of these coeval gases can contribute significantly to the overpressure necessary to form large deep-water pyroclastic eruptions, as proposed by Svensen et al. (2004) and Agirrezabala et al. (2017) for example.

Given the uncertainties and limitations of using small cutting samples from borehole data, it was not possible to confidently interpret the origin of the volcaniclastics rocks as primary eruptive or resedimented deposits. Some volcanic textures (rounded clasts and polymictic material) together with volcaniclastic material occurring mixed with the Tokama Siltstone, suggest some degree of reworking of these deposits. However, mixing of volcaniclastics and siliciclastic material may be caused by drilling issues or could represent the distal products of submarine pyroclastic plumes that incorporated lithics from the Tokama Siltstone during magma fragmentation and transport (White 2000). In contrast, wireline-logs of Resolution-1 show sharp log-facies contacts at the boundaries between volcaniclastics and siltstones (Figure 6), which commonly indicate abrupt compositional changes in lithofacies and could point towards a primary volcaniclastic deposit. In addition, seismic facies corresponding to the volcaniclastic interval show constant lateral thickness and are not confined to valleys (Figure 14), a characteristic of subaerial pyroclastic surge deposits (Cas and Wright 1992). This constant lateral thickness may indicate similar processes to those observed in deposits of eruption-fed density currents (White 2000). These observations reinforce the view that both end members, primary and reworked volcaniclastics, could be present in Resolution-1. In light of these uncertainties, integration of petrography, seismic stratigraphy and biostratigraphic data indicate that these volcaniclastic rocks were: i) erupted onto sediments deposited in a deep-water setting (ca 1000 to 1500 m), ii) likely experienced pyroclastic and possibly autoclastic fragmentation, iii) may or may not have been reworked, and iv) deposited next to the volcanoes pc14, nf02 and nf03 (Figure 4 and 15). These evidences suggest that volcaniclastic rocks of association V may represent volcanogenic deposits erupted from diverse volcanoes. Although some of the volcanic textures more likely indicate a pyroclastic origin, their analysis alone could not provide enough evidence to define the MVF past-eruptive styles. Insights from seismic reflection data enriched these interpretations.

Conclusions

Volcaniclastic and intrusive rocks collected from the Resolution-1 well confirm a magmatic origin of the anomalies observed in seismic lines in the study area. In seismic imagery, these volcanic anomalies form a cluster of middle Miocene volcanoes and correlative intrusive bodies, here referred as the Maahunui Volcanic Field (MVF). Integration of the results from this and previous work suggests that magmatic activity in MVF was active from ca 12.7 to 11.5 Ma. The magmatic products representative of MVF melts are primarily alkalic basalts in composition. Miarolitic cavities and ophitic texture observed in the monzogabbro penetrated by Resolution-1 indicate that the saucer-shaped intrusion imaged in seismic lines was injected at shallow depths of ca 950 m below the middle Miocene MVF paleo-sea floor. Integration of petrographic, geochemical and seismic interpretation indicate that the volcaniclastic rocks likely have a genetic relationship with the saucer-shaped monzogabbro. This shallow intrusive body possibly served as a stationary magma chamber that fed eruptions onto the middle Miocene paleo-seafloor. Biostratigraphic data suggest that these eruptions occurred in a lower bathyal setting (1000 - 1500 m depth) in the vicinity of Resolution-1. High contents of glass shards, relics of bubble walls, presence of spheroidal aggregates enveloped in palagonite films (possibly armoured lapilli), broken phenocrysts, and lithics, suggest possible pyroclastic mechanisms of fragmentation. This interpretation is supported by the seismic morphology of the volcanoes in the MVF, which indicate material fragmentation and particle dispersion comparable to those produced by phreatomagmatic eruptions, although this eruptive style is rarely considered to occur in deep-waters (ca 1000 m). The emplacement of intrusive bodies into organic-rich sedimentary rocks of the Broken River Formation could incorporate thermogenic gases into the magmatic system, contributing with the overpressure necessary to form large deep-water pyroclastic eruptions. This study demonstrates the value of combining insights from petrographic analysis with seismic reflection interpretation to investigate the formation of ancient volcanoes now buried in sedimentary basins.

List of tables

Table 1: Main stratigraphic and paleoenvironmental characteristics of Rock Association IV. The highlighted middle Tokama depositional unit (red) is interbedded with the volcaniclastic rocks of the MVF. These rocks were deposited in a lower bathyal setting (1500-1000 m water depths).

Depositional unit	Depth in the well	Age	Depositional setting	Lower bound	Upper bound	Thickness (m)
Uppermost Tokama	1016 to 686.1	Late-early Miocene to late Pliocene	Uppermost bathyal	Unc. lM	Unc. eP	329.9
Upper Tokama	1070 to 1016	Late-early Miocene	Mid bathyal	Onset of slope progradation	Unc. lM	54
Middle Tokama	1269 to 1070	Middle Miocene	Lower bathyal (1500-1000 m)	Unc. eM	Onset of slope progradation	190
Lower Tokama	1284.1 to 1269	Late-early Miocene	Deep-lower bathyal	Omihi Fm	Unc. eM	24

List of figures

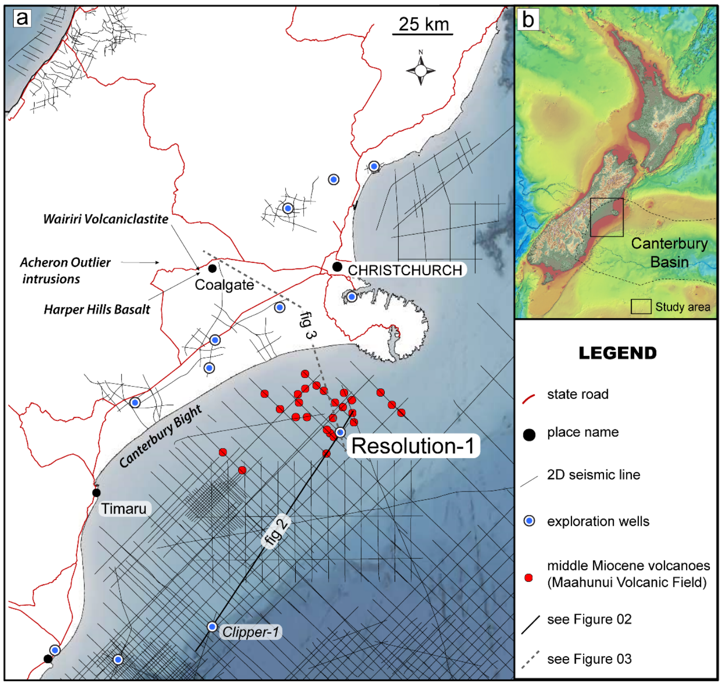

Figure 1: a) Map showing the location of volcanoes of the MVF (red dots) mapped from 2D seismic reflection lines (thin black lines). b) New Zealand topographic and bathymetric map (NZ Petroleum Exploration 2018 datapack) showing the location of the study area.

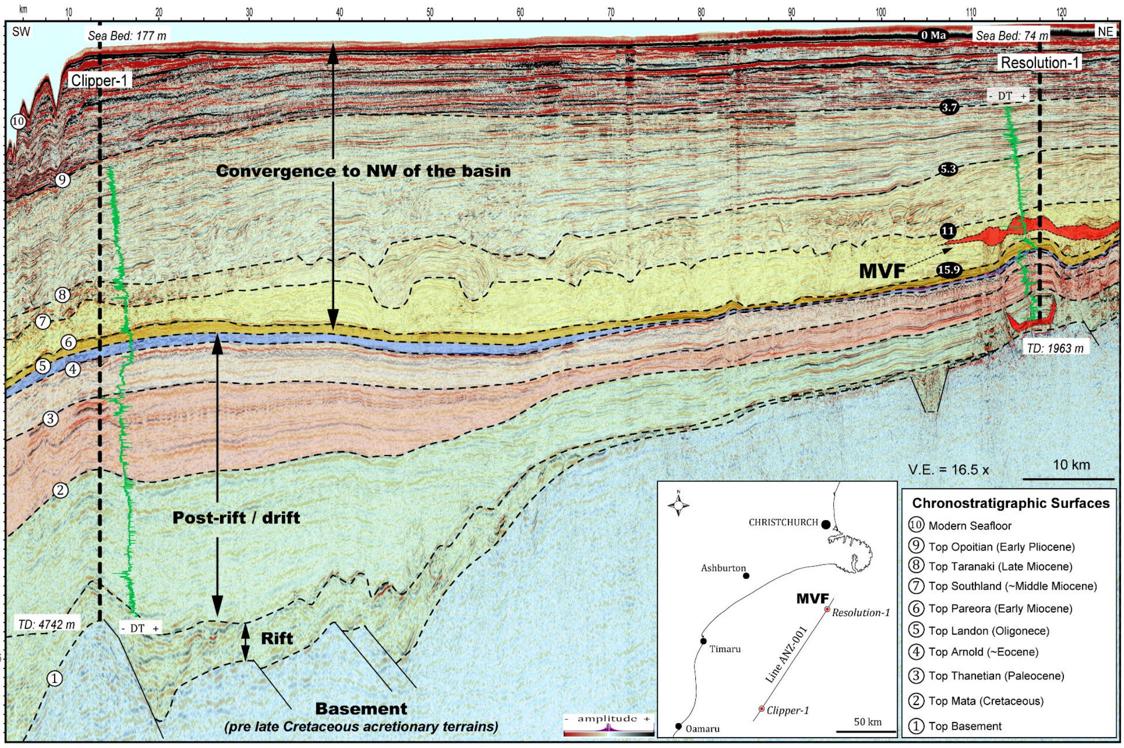

Figure 2: 2D regional strike/oblique seismic line showing the location of the MVF (red) and its location in the basin succession. The Resolution-1 and Clipper-1 wells were used to tie the seismic data to chronostratigraphic surfaces (1 to 10) that represent important changes during the evolution of Canterbury Basin.

522

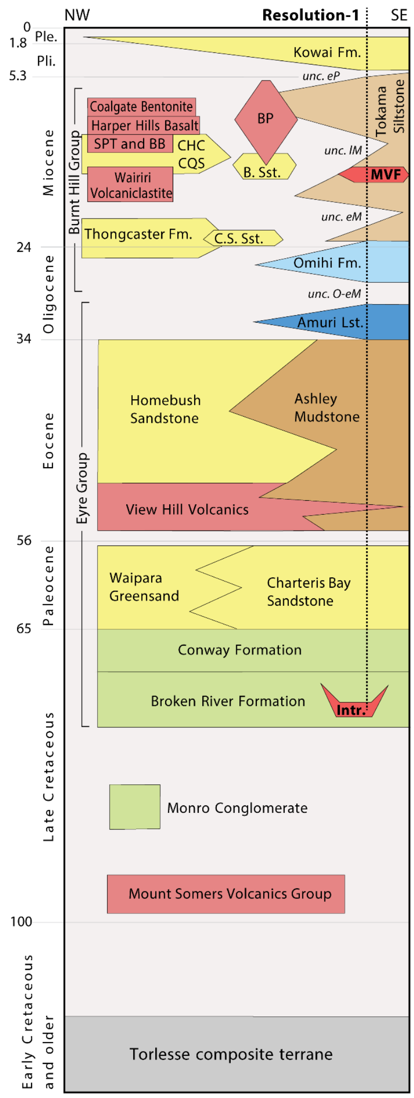

523 Figure 3: Simplified Cretaceous and Cenozoic chronostratigraphic chart of the northern
524 Canterbury Basin. Abbreviations are: middle Miocene monzogabbro intrusion (Intr.),
525 Curiosity Shop Sandstone (C.S. Sst.), Bradley Sandstone (B. Sst.), Chalk Quarry
526 Sandstone (CQS), Chalk Hill Clay (CHC), Maahunui Volcanic Field (MVF), Banks
527 Peninsula volcanics (BP), Sandpit Tuff (SPT) and Bluff Basalt (BB). Age of
528 unconformities in the Resolution-1 well are: Oligocene-early Miocene (O-eM), early
529 Miocene (eM), late Miocene (lM) and early Pliocene (eP). After Carlson et al. (1980),
530 Field et al. (1989), Forsyth et al. (2008), Schiøler et al. (2011) and Boyes et al. (2012).

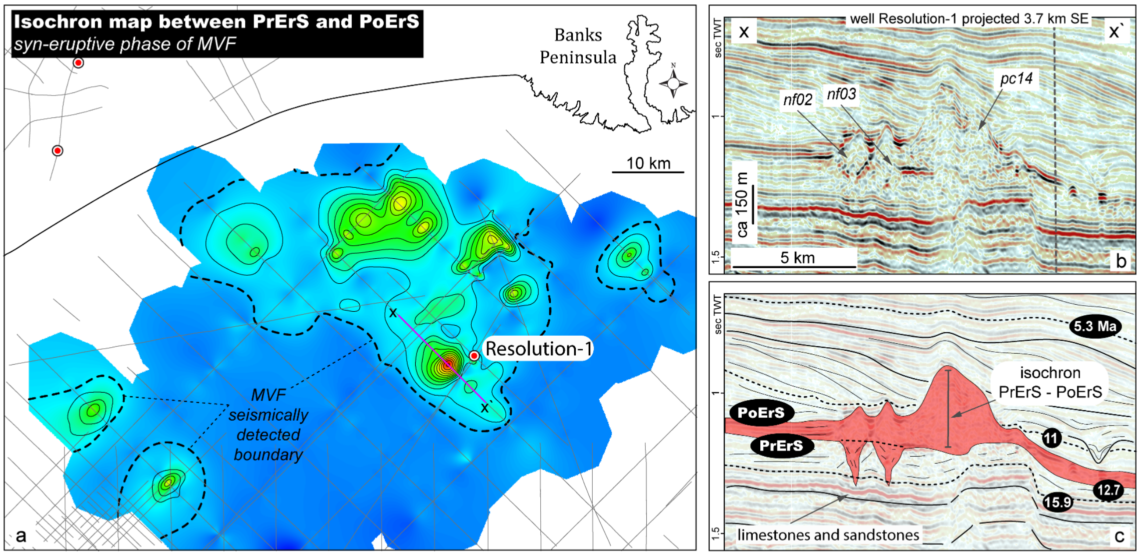

Figure 4: a) Isochron map between pre-eruptive (PrErS) and post-eruptive surfaces (PoErS) of the MVF showing the locations of cone-type volcanoes. Note that the surfaces thin and amalgamate with increasing distance from individual or clusters of volcanoes, defining the seismic detectable boundaries of the MVF. (b) Uninterpreted and (c) interpreted seismic line across volcanos pc14, nf02 and nf03. Negative structures (nf02 and nf03) were excluded during mapping of the PrErS surface due to computer limitations, as they would have shown a false positive structure on the isochron map.

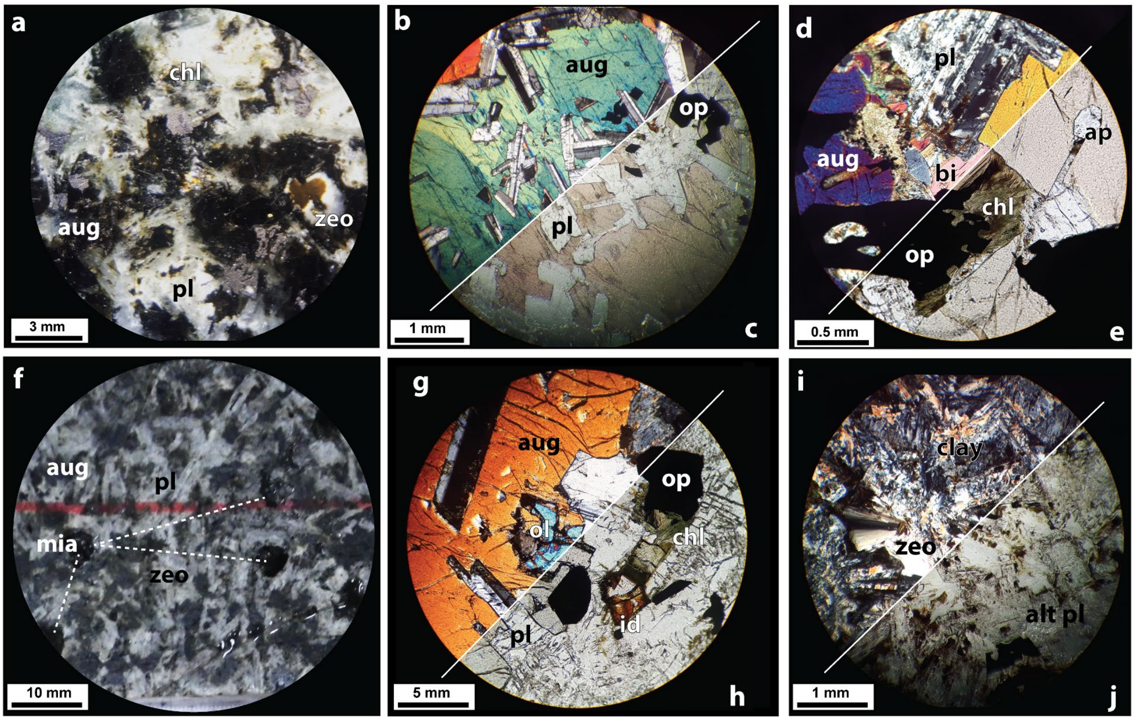

Figure 5: (a and f) Medium-grained monzogabbro recovered from a depth of 1962.25 m, showing plagioclase (pl), pyroxene (aug), chlorite (chl), zeolite (zeo) and miarolitic cavities (mia). (b, d, g and i) Thin-sections in cross-polarized light showing ophitic texture of plagioclase and augite, olivine (ol) crystals partially replaced by iddingsite (id), augite replaced by biotite (bi) and chlorite, radial zeolite filling interstitial space and plagioclase replaced by clays (alt pl). Accessory minerals are opaques (op) and apatite (ap). (c, e, h and j) show the same thin sections in plain-polarized light.

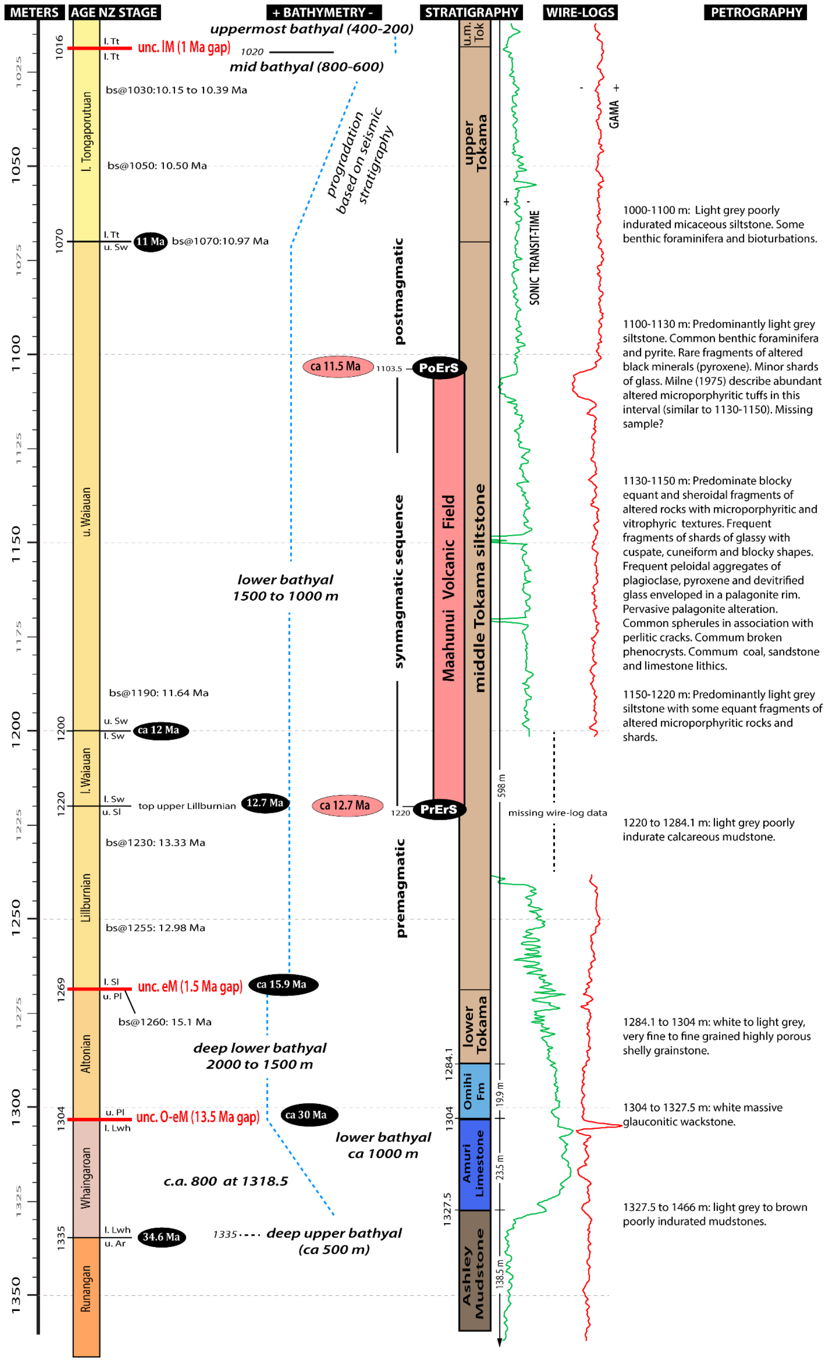

Figure 6: Composite data of the Oligocene-Miocene interval of the Resolution-1 well showing the lithologies, ages, paleoenvironments, stratigraphy, and wire-logs. Symbols "bs@" give the biostratigraphic age of Schiøler et al. (2011). Blue dashed lines show the bathymetric trend. Numbers in black ellipses are ages derived using the 2015 NZ Geologic Time Scale (Raine et al. 2015). Numbers in red ellipses are estimated ages of the MVF based on the integration of insights from seismic reflection lines with radiometric dating of igneous rocks representative of the MVF, and biostratigraphy analysis of the enclosing sedimentary strata.

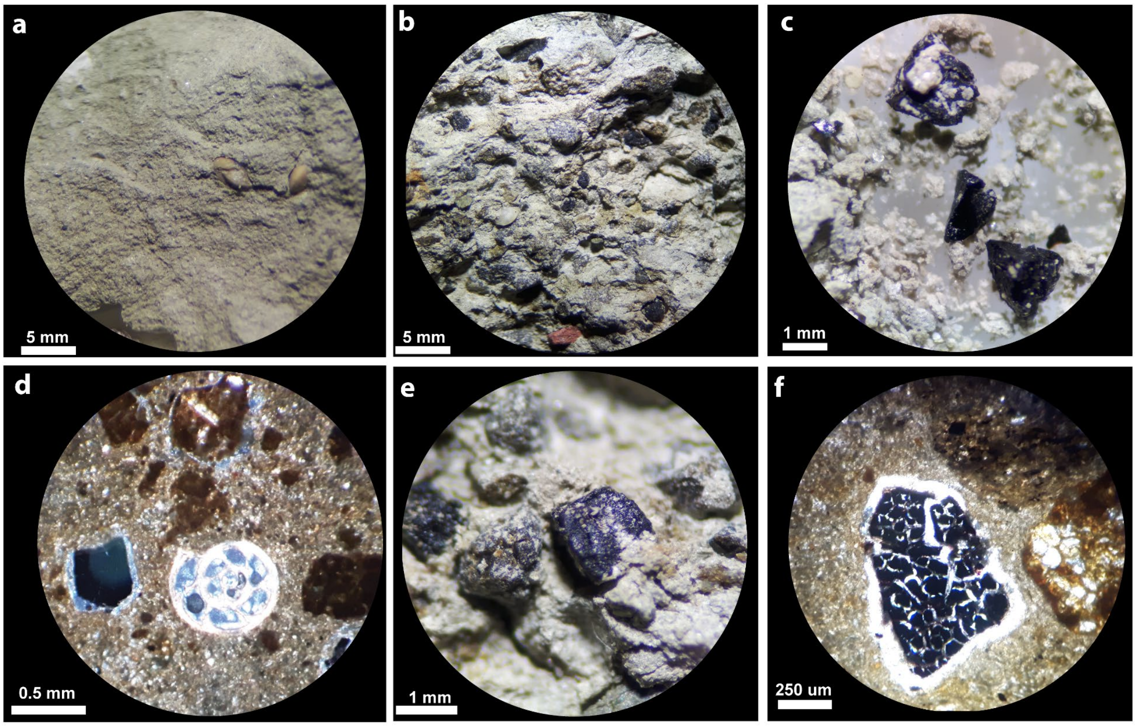

Figure 7: (a) Unwashed cutting samples of the middle Tokama depositional unit (Rock Association IV) recovered from the interval 1130 to 1120 m showing a massive siltstone with foraminifer fossils. (b, c and e) Unwashed cutting samples of the Rock Association V (1140-1130 m) showing volcanic fragments, coal lithics, bioclasts, and altered crystals of pyroxenes (detailed in e). Thin section in cross-polarized light (d) and plain-polarized light (f) showing an unwashed cutting sample comprising a gastropod fossil, coal lithics, and volcanic fragments with pervasive palagonite alteration.

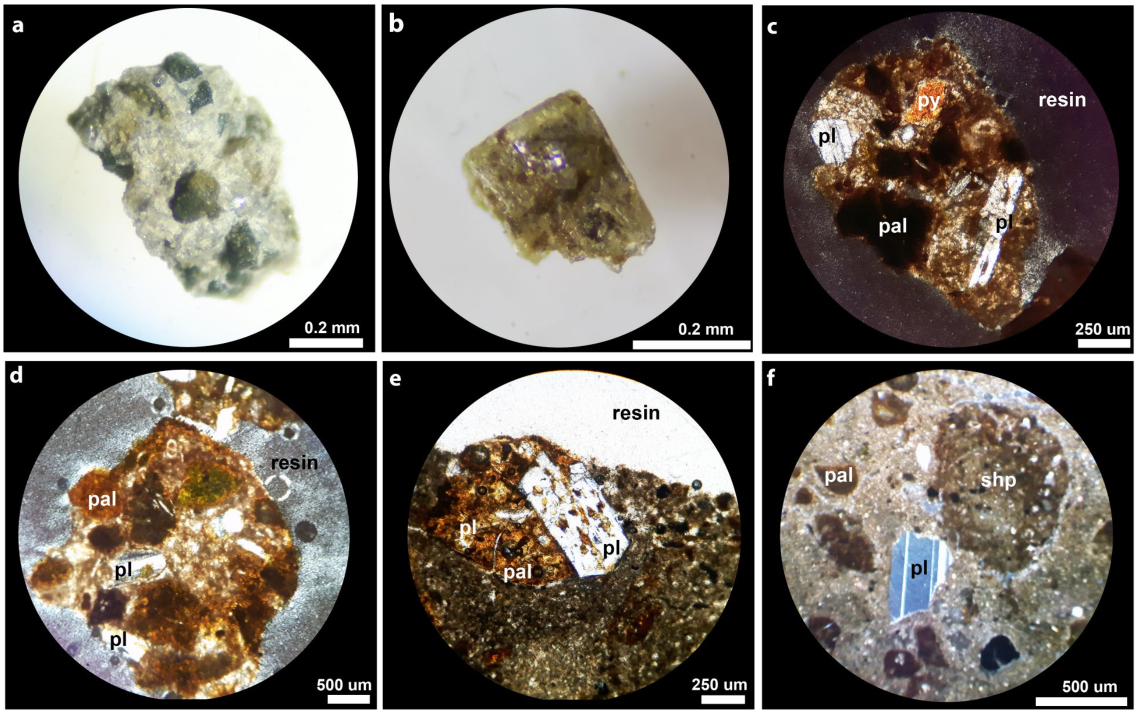

Figure 8: Washed (a to d) and unwashed (e and f) cutting samples of Rock Association V collected from the depths of 1140 to 1130 m in Resolution-1. (a) A loose fragment of an aggregate of plagioclase (pl) and pyroxene (py) phenocrysts. (b) An example of a broken plagioclase fragment. (c to e) Thin sections in cross-polarized and plain-polarized light (e) showing volcaniclastic fragments with microporphyritic and vitrophyric textures. Note the plagioclase with rounded borders (d) and the anhedral broken crystals (c and f). Fragments with spherical shapes (shp) are commonly observed in the Rock Association V (f).

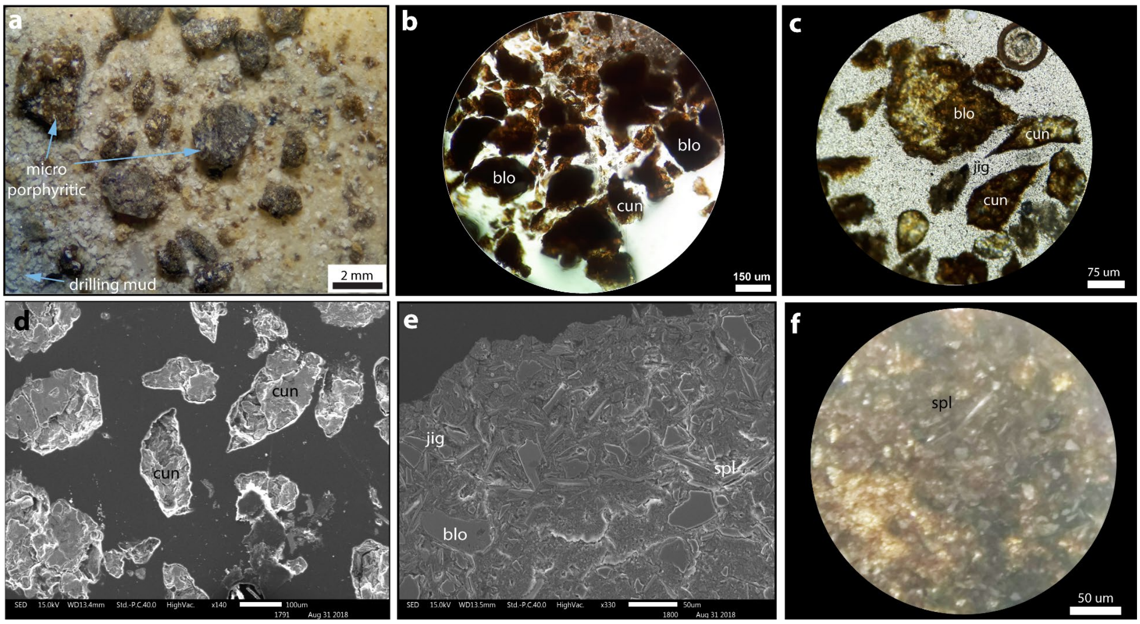

Figure 9: Washed cutting samples of the Rock Association V collected from the depths of 1140 to 1130 m in Resolution-1. (a) Well cuttings submerged in water during the washing process showing altered blocky equant volcaniclastic fragments with microporphyritic texture. Thin sections in plain-polarized light (b, c and f) and SEM images (d and e) showing spalls of glassy shards with cuneiform (cun), blocky (blo) and splintery (spl) shapes within a jigsaw-fit (jig) texture.

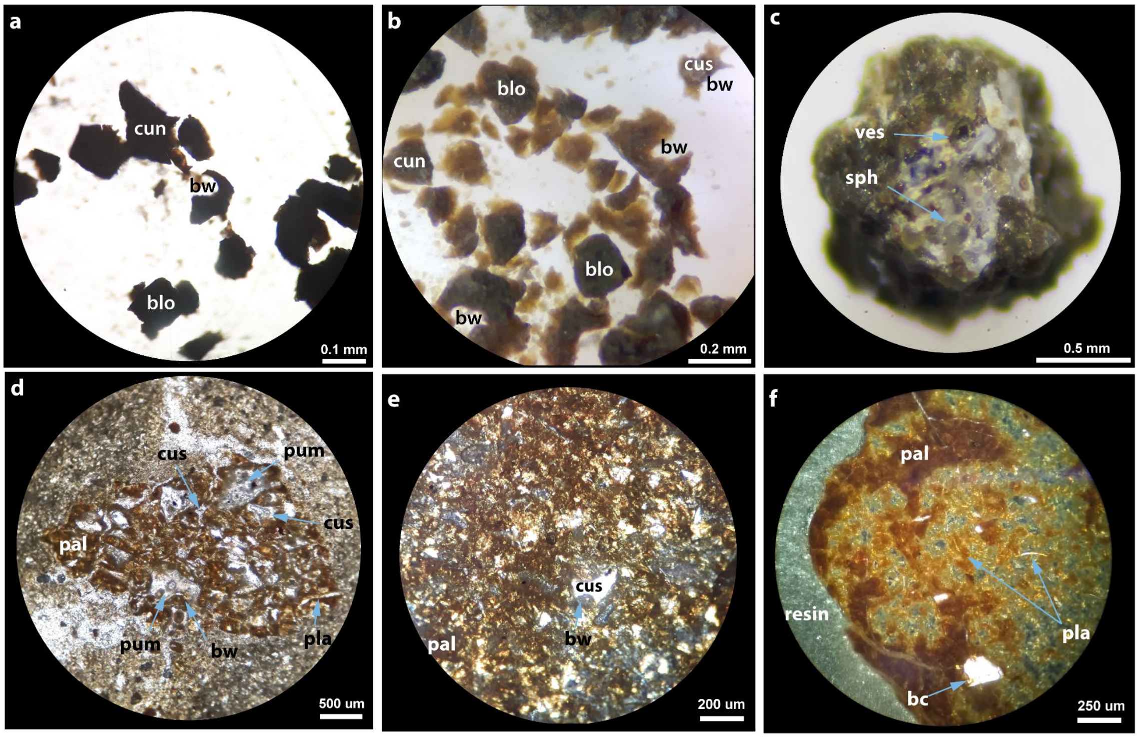

Figure 10: Washed cutting samples of the Rock Association V collected from the depths of 1130 to 1140 m in Resolution-1. (a, b and c) Loose fragments of shards with cuspate (cus), cuneiform (cun), blocky (blo) and platy (pla) shapes, relic bubble walls (bw), spherules (sph) and vesicles (ves). Thin sections in cross-polarized (d and e) and plain-polarized light (f) showing shards with cuspate, platy and pumice (pum) shapes in association with fragments of broken crystals (bc) and pervasive palagonite (pal) alteration.

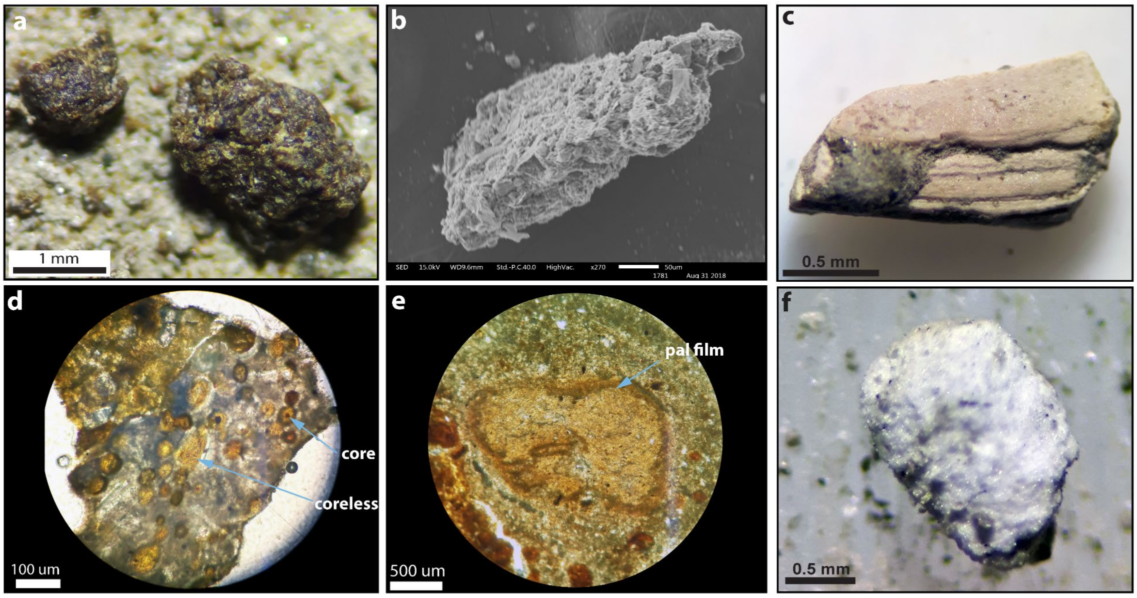

Figure 11: Washed cutting sample (a) and SEM image (b) of loose, poorly-indurated aggregates of microcrystals and sharp fragments of glass from the interval 1140 to 1130 m in Resolution-1. Thin-sections in plain-polarized (d) and cross-polarized (e) light showing core (possible a lithic fragment) and coreless fragments with a spherical shape enveloped in a palagonite (pal) film. Loose limestone (c) and sandstone (f) fragments collected from the interval of 1140 to 1130 m. These rocks are lithics found within the volcaniclastics of the Rock Association V, and are petrographically similar to the underlying limestones and sandstones of Rock Associations II and III.

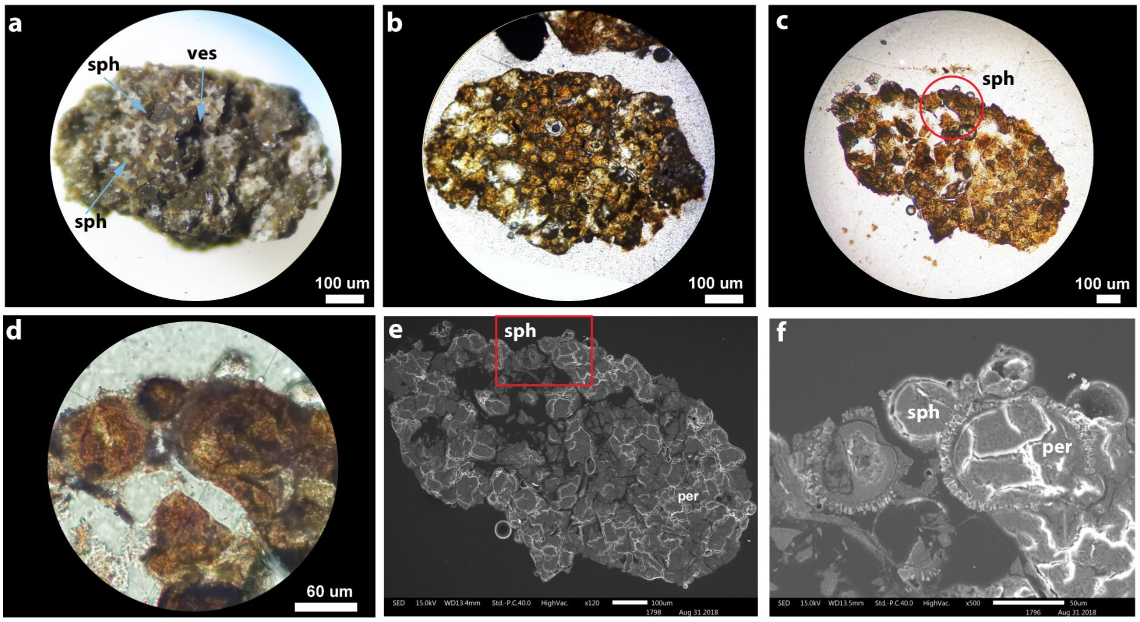

Figure 12: Washed cutting sample (a) from the interval 1130 to 1140 m showing well-indurated spherules (sph) and vesicles (ves). (b and c) Thin-sections in plain-polarized light and (d), cross-polarized light, and (e and f) SEM. These spherules contain a devitrified (palagonite) inner core, a single concentric outer rim, and an external array of acicular crystals in a radial pattern, typically associated with perlitic cracks (per). Detail of the red circle highlighted in (c) is shown in (d). Detail of the red square in (e) is shown in (f). Pervasive alteration to palagonite is common.

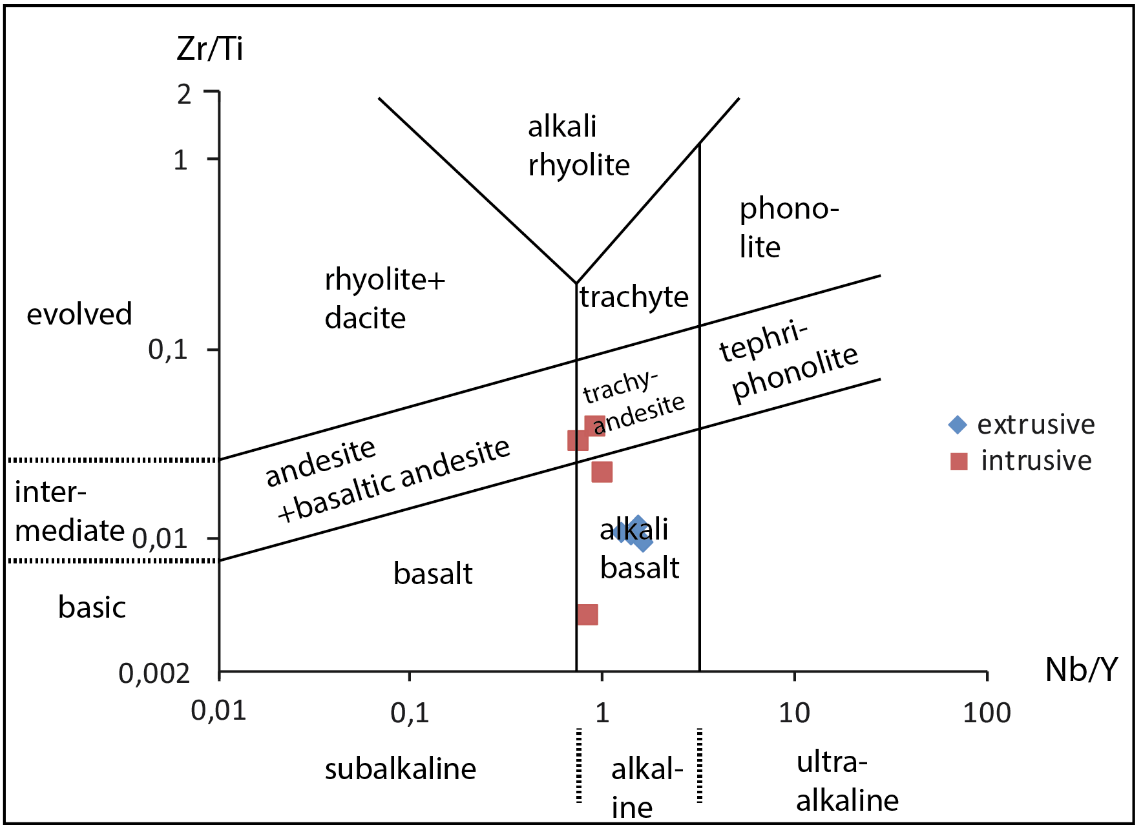

Figure 13: Zr/Ti versus Nb/Y diagram (Pearce 1996 after Winchester and Floyd 1977), used to compare the composition of the igneous rocks sampled in Resolution-1. Both extrusive and intrusive rocks plot in the alkaline series suggesting a possible co-genetic relationship of these rocks, which is reinforced by analysis of seismic reflection lines in the vicinity of the well (Figure 14 and 15).

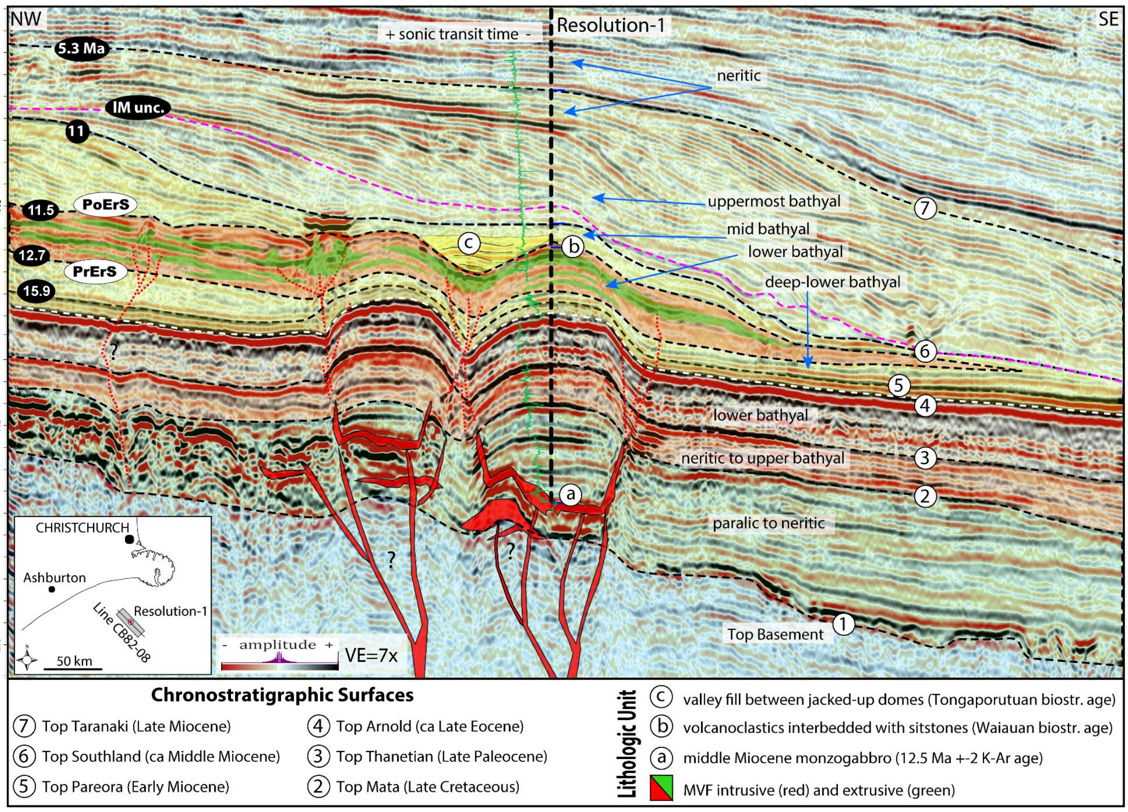

Figure 14: Interpreted 2D dip seismic section at the location of Resolution-1 (thick dashed line). Saucer-shaped sills (a) were intruded into Cretaceous sedimentary strata during the Miocene (12.5 ± 2 Ma K-Ar date). The syn-eruptive interval (between PrErS and PoErS) is defined by the occurrence of volcaniclastic rocks (b) interbedded with the Tokama Siltstone of Waiauan age (ca 12.7 to 11 Ma). The emplacement of these intrusions caused doming of the overlying strata, consequentially changing the paleo-sea floor topography and promoting deposition of channelized systems (c) next to the dome structures during the late Waiauan (11.5 to 11 Ma).

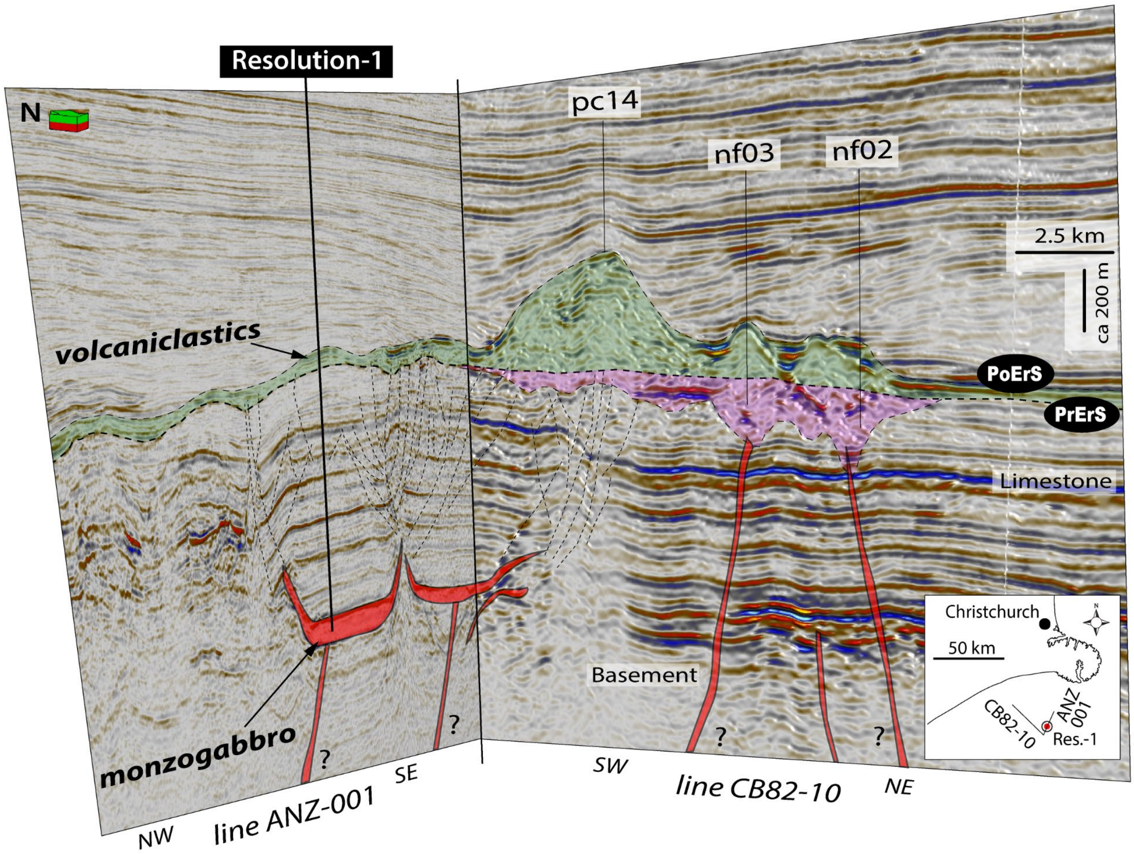

Figure 15: Interpreted 2D composite section at the location of Resolution-1 showing the seismic expression of the shallow plumbing system and the morphology of some of the volcanoes in the MVF. Note the array of faults at the tips of the saucer-shaped intrusions, which possibly aided pathways for magma and hydrothermal fluids migrate up-sequence. Note that the extension of these faults connects the saucer-shaped intrusions (bottom) with the root of the volcano pc14 (top), suggesting a feeding system for eruptions onto the Miocene paleo-sea bed. The zone highlighted in purple below the volcanoes pc14, nf02 and nf03 is interpreted to correspond with craters excavated into the pre-eruptive surface.

List of appendixes

	SiO_2	Al_2O_3	MgO	Fe_2O_3	CaO	K_2O_5	P_2O_5	TiO_2	MnO	Total	Ti	Y	Zr	Nb	Nb/Y	Zr/Ti
Int_s1	45,50	17,38	3,74	12,10	4,66	1,64	0,45	2,33	0,13	87,93	13942	22,4	304,6	23,3	1,040	0,022
Int_s2	48,44	17,98	4,82	11,97	6,21	1,76	0,80	1,39	0,13	93,49	8358	24,4	323	23	0,943	0,039
Int_s3	55,86	20,09	4,37	7,95	8,38	1,45	0,14	1,09	0,11	99,44	6562	22,4	210,4	17,4	0,777	0,032
Int_s4	47,65	15,27	6,68	8,66	12,90	0,34	0,14	4,82	0,12	96,58	28878	14,9	111,6	12,8	0,859	0,004
Ext_s1	54,93	16,59	5,47	20,93	10,35	2,85	0,53	4,64	0,29	116,59	27824	43,6	297,8	61,4	1,408	0,011
Ext_s2	48,03	13,96	5,74	22,53	13,49	1,76	0,56	4,77	0,39	111,23	28587	38,1	279,8	61,3	1,609	0,010
Ext_s3	45,07	14,74	4,97	19,16	13,42	2,13	0,71	3,78	0,36	104,33	22655	44,8	245,2	56,2	1,254	0,011
Ext_s4	40,81	13,54	4,07	15,62	11,89	1,80	0,49	3,10	0,29	91,61	18595	31,9	221,4	49,1	1,539	0,012

Appendix 1: XRF results from Rock Association I (intrusive) and Rock Association V (extrusive) of Resolution-1. Sn correspond to the number of shots given in each sample. Major elements are presented in weight percent (wt%), while incompatible elements are in parts per million (ppm).

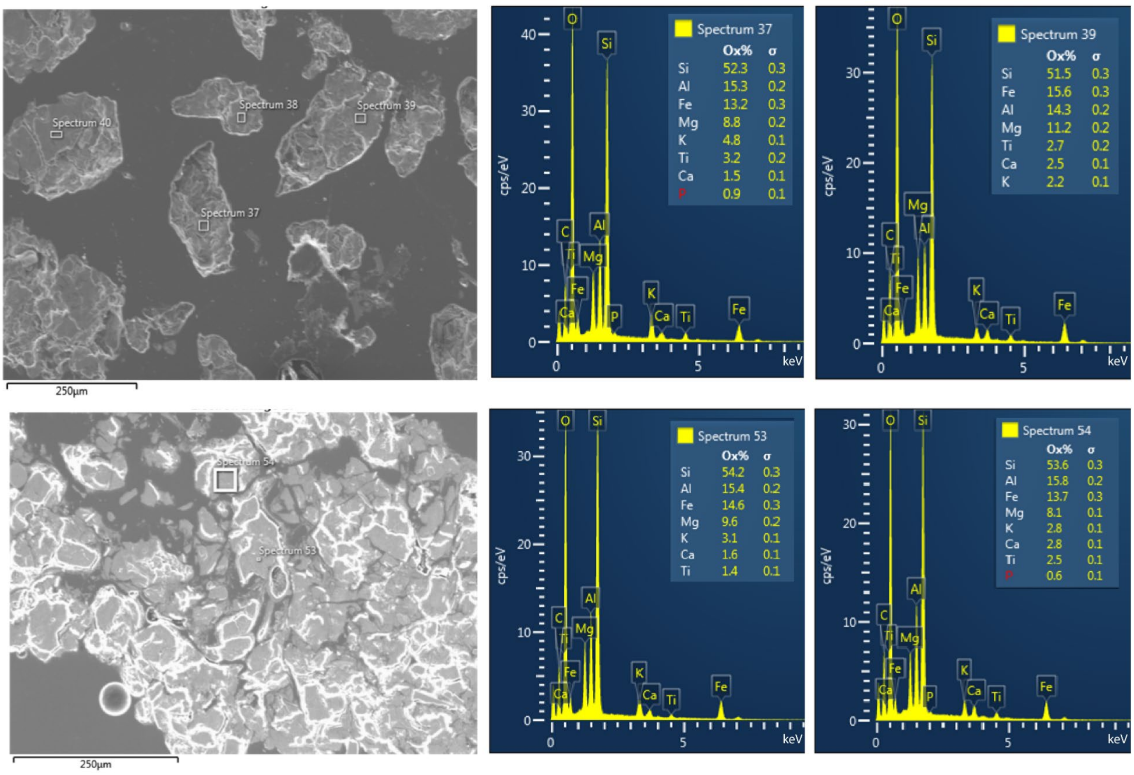

Appendix 2: Results from EDS analysis of volcanic glass from Rock Association V.

Acknowledgments

We would like to thank IHS Markit and Schlumberger for providing academic licence to use the Kingdom and Petrel software, and the NZPM for providing the dataset for this study. Thanks to Jane Newman for the petrographic insights, to Simon Holford and Sverre Planke for their excellent reviews of the manuscript, and to Judy Fierstein for helping to improve this paper.

References

Aarnes I, Planke S, Trulsvik M, Svensen H (2015) Contact metamorphism and thermogenic gas generation in the Vøring and Møre basins, offshore Norway, during the Paleocene-Eocene thermal maximum. J Geol Soc 172: 588-598

Agirrezabala L, Sarrionandia F, Carracedo M (2017) Diatreme-forming volcanism in a deep-water faulted basin margin: Lower Cretaceous outcrops from the Basque-Cantabrian Basin, western Pyrenees. J Volcanol Geotherm Res. https://doi.org/10.1016/j.jvolgeores.2017.03.019

Arnórsson S, Thórhallsson S, Stefánsson A (2015) Utilization of Geothermal Resources, in The Encyclopedia of Volcanoes. https://doi.org/10.1016/B978-0-12-385938-9.00071-7

Barrier, A., 2019. Tectonics, Sedimentation and Magmatism of the Canterbury Basin, New Zealand. Ph.D. Thesis, Canterbury University, New Zealand.

Barrier A, Nicol A, Bischoff AP (2017) Volcanism Occurrences in the Canterbury Basin, New Zealand and Implication for Petroleum Exploration. In AAPG GTW Influence of Volcanism and Associated Magmatic Processes on Petroleum Systems. Conference, Oamaru New Zealand.

Best MG, Christiansen EH (1997) Origin of broken phenocrysts in ash-flow tuffs. Geol Soc Am Bull. https://doi.org/10.1130/00167606(1997)109<0063:OOBPIA>2.3.CO;2

Bischoff AP, Nicol A, Barrier A, Beggs M (2016) The Stratigraphic Record of Volcanism - Examples from New Zealand Sedimentary Basins. In 2016 Geoscience Society of New Zealand Conference, Wanaka, Abstract.

Bischoff AP, Nicol A, Beggs M (2017) Stratigraphy of architectural elements in a buried volcanic system and implications for hydrocarbon exploration: Interpretation. https://doi.org/10.1190/INT-2016-0201.1

Bischoff AP (2019) Architectural Elements of Buried Volcanic Systems and Their Impact on Geoenergy Resources. Ph.D. Thesis, Canterbury University, New Zealand. Pre-print, pp 226. 10.13140/RG.2.2.21440.58886

Bischoff AP, Nicol A, Barrier A, Wang H (2019a) Seismic Morphological and Paleogeographic Reconstruction of Buried Monogenetic Volcanic Field. Online pre-print in EarthArXiv. Submitted to the Bulletin of Volcanology. 10.31223/osf.io/3yrcu

Bischoff AP, Nicol A, Cole J, Gravley D (2019b) Stratigraphy of Architectural Elements of a Buried Monogenetic Volcanic System and Implications for Geoenergy Exploration. Online pre-print in EarthArXiv. Submitted to the Open Geosci. 10.31223/osf.io/h9zuq

Blanke SJ (2010) “Saucer Sills” of the Offshore Canterbury Basin: GNS Publication. https://doi.org:10.1177/0094306114545742f

Browne GH (1983) A new interpretation of brecciation in the sandpit tuff, harper hills, Canterbury. New Zeal J Geol Geophys. https://doi.org/10.1080/00288306.1983.10422258

Carlson JR, Grant-Mackie JA, Rodgers KA (1980) Stratigraphy and sedimentology of the coalgate area, Canterbury, New Zealand: New Zeal J Geol Geop. https://doi.org/10.1080/00288306.1980.10424205

Cas RA, Wright FJV (1993) Volcanic Successions: Modern and Ancient - A Geological Approach to Processes, Products and Successions. Chapman and Hall, UK. https://doi.org:10.1007/978-0-412-44640-5

Cas RA, Giordano FG (2014) Submarine volcanism: A review of the constraints, processes and products, and relevance to the Cabo de Gata volcanic succession. https://doi.org:10.3301/IJG.2014.46

Catuneanu O (2006) Principles of Sequence Stratigraphy. Changes, 375. https://doi.org:10.5860/CHOICE.44-4462

Coombs DS, White AJR, Hamilton D, Couper RA (1960) Age relations of the Dunedin volcanic complex and some paleogeographic implications—Part II: New Zeal J Geol Geop. https://doi.org:10.1080/00288306.1960.10420145

Coombs DS, Cas RA, Kawachi Y, Landis CA, McDonough WF, Reay A (1986) Cenozoic volcanism in north, east and central Otago. In: Smith IEM (ed) Late Cenozoic Volcanism in New Zealand. R Soc New Zeal Bull 23: 278-312

Delmelle P, Maters E, Oppenheimer C (2015) Volcanic Influences on the Carbon, Sulfur, and Halogen Biogeochemical Cycles. In: Sigurdsson H, Houghton B, McNutt S, Rymer H, Stix J (eds) Encyclopedia of Volcanoes. Academic Press, New York. https://doi.org/10.1016/B978-0-12-385938-9.00050-X

Eady AE (1995) The Petrology and Geochemistry of the Acheron Intrusion. MSc Thesis, Canterbury University pp 183. http://hdl.handle.net/10092/6783

Field BD, Browne GH, Davy BW, Herzer RH, Hoskins RH, Raine JI, Wilson GJ, Sewell RJ, Smale D, Watters WA (1989) Cretaceous and Cenozoic sedimentary basins and geological evolution of the Canterbury region, South Island, New Zealand. Lower Hutt: New Zealand Geological Survey. New Zealand Geological Survey Basin Studies 2: 94.

Finn CA, Müller RD, Panter KS (2005) A Cenozoic diffuse alkaline magmatic province (DAMP) in the southwest Pacific without rift or plume origin. Geochem Geophys Geosy. https://doi.org/10.1029/2004GC000723

Forsyth PJ, Barrell D.J.A, Jongens R (2008) Geology of the Christchurch area. Institute of Geological and Nuclear Sciences 1:250,000 Geological Map 16. Lower Hutt, GNS Science. 67 p1 sheet.

Giba M, Walsh JJ, Nicol A, Mouslopoulou V, Seebeck H (2013) Investigation of the Spatio-Temporal Relationship between Normal Faulting and Arc Volcanism on Million-Year Time Scales. J Geol Soc 170: 951–962. https://doi.org/10.1144/jgs2012-121

Graettinger AH, Valentine GA, Sonder I (2016) Recycling in Debris-Filled Volcanic Vents. Geology 44: 811. https://doi.org/10.1130/G38081.1

Hawkes PW, Mound DD (1984) BP Shell Todd (Canterbury) Services Limited, Clipper-1 Geological Completion Report PR1036.

Holford SP, Schofield N, MacDonald JD, Duddy IR, Green PF (2012) Seismic Analysis of Igneous Systems in Sedimentary Basins and Their Impacts on Hydrocarbon Prospectivity: Examples from the Southern Australian Margin. APPEA Journal, 52: 229–252.

Hunt D, Tucker ME (1992) Stranded parasequences and the forced regressive wedge systems tract: deposition during base-level fall: Sediment Geol 81: 1–9. https://doi.org/10.1016/0037-0738(92)90052-S

Huafeng T, Phiri C, Youfeng G, Yulong H, Weihua, B (2015) Types and Characteristics of Volcanostratigraphic Boundaries and Their Oil-Gas Reservoir Significance. Acta Geologica Sinica - English Edition, 89: 163-174. https://doi.org/10.1111/1755-6724.12402

Iacono-Marziano G, Morizet Y, Le Trong E, Gaillard F (2013) New experimental data and semi-empirical parameterization of H2O-CO2 solubility in mafic melts. Geochimica Et Cosmochimica Acta 97: 145-157

Infante-Paez L, Marfurt KJ (2017) Seismic expression and geomorphology of igneous bodies: A Taranaki Basin, New Zealand, case study: Interpretation, 5, no. 3, p. SK121-SK140, https://doi.org/10.1190/INT-2016-0244.1

Jerram DA, Single RT, Hobbs RW, Nelson CE (2009) Understanding the offshore flood basalt sequence using onshore volcanic facies analogues: An example from the Faroe-Shetland basin. Geol Mag. https://doi.org/10.1017/S0016756809005974

Kamp PJJ, Green PF, Tippett JM (1992) Tectonic architecture of the mountain front-foreland basin transition, South Island, New Zealand, assessed by fission track analysis. Tectonics. https://doi.org/10.1029/91TC02362

Kereszturi G, Németh C (2013) Monogenetic Basaltic Volcanoes: Genetic Classification, Growth, Geomorphology and Degradation: Updates in Volcanology - New Advances in Understanding Volcanic Systems, https://doi.org/10.5772/51387

Lever H (2007) Review of unconformities in the late Eocene to early Miocene successions of the South Island, New Zealand: Ages, correlations, and causes: New Zeal J Geol Geophys 50: 245-261

Lu H, Fulthorpe CS, Mann P, Kominz MA (2005) Miocene-Recent tectonic and climatic controls on sediment supply and sequence stratigraphy: Canterbury basin, New Zealand: Basin Res 17: 311–328. https://doi.org/10.5772/5138710.1111/j.1365-2117.2005.00266.x

Lorenz V (1985) Maars and diatremes of phreatomagmatic origin, a review. Transactions of the Geological Society of South Africa 88: 459-470.

Marfurt K (2018) Seismic Attributes as the Framework for Data Integration Throughout the Oilfield Life Cycle: Society of Exploration Geophysicists pp 508. https://doi.org/10.1190/1.9781560803522

McPhie J, Doyle M, Allen R (1993) Volcanic textures - a guide to the interpretation of textures in volcanic rocks. Centre for Ore Deposit and Exploration Studies, University of Tasmania.

McLean CE, Schofield N, Brown DJ, Jolley DW, Reid A (2017) 3D seismic imaging of the shallow plumbing system beneath the Ben Nevis Monogenetic Volcanic Field: Faroe–Shetland Basin: J Geol Soc. https://doi.org/10.1144/jgs2016-118

Magee C, Murray H, Christopher JAL, Stephen JM (2019) Burial-Related Compaction Modifies Intrusion-Induced Forced Folds: Implications for Reconciling Roof Uplift Mechanisms Using Seismic Reflection Data. Front Earth Sci. doi:10.3389/feart.2019.00037

Milne AD (1975) Well completion report Resolution, for BP, Shell, Todd Canterbury Service Limited. New Zealand Geological Survey Open-file Petroleum Report No. 648.

Mortimer N (2004) New Zealand's Geological Foundations: Gondwana Research, v. 7, no. 1, p. 261-272.

Pearce TH (1993) Analcime phenocrysts in igneous rocks: Primary or secondary? Discussion. Am Mineral 78: 225-229.

Pearce JA (1996) A users guide to basalt discrimination diagrams. In: Wyman DA (eds). Trace Element Geochemistry of Volcanic Rocks: Applications for Massive Sulphide Exploration. Short Course Notes 12. St. John’s, Canada: Geological Association of Canada, pp 79-113

Peretyazhko IS (2010) Genesis of mineralized cavities (Miaroles) in granitic pegmatites and granites. Petrol. https://doi.org/10.1134/S0869591110020062

Planke S, Alvestad E, Eldholm O (1999) Seismic Characteristics of Basaltic Extrusive and Intrusive Rocks. The Leading Edge 18: 342. https://doi.org/10.1190/1.1438289

Planke S, Symonds PA, Alvestad E, Skogseid J (2000) Seismic Volcanostratigraphy of Large-Volume Basaltic Extrusive Complexes on Rifted Margins. J Geophys Res 105 (B8): 19335. https://doi.org/10.1029/1999JB900005

Planke S, Millett JM, Maharjan D, Jerram DA, Abdelmalak MM, Groth A, Hoffmann J, Berndt C, Myklebust R (2017) Igneous seismic geomorphology of buried lava fields and coastal escarpments on the Vøring volcanic rifted margin: Interpretation. https://doi.org/10.1190/INT-2016-0164.1

Reynolds P, Schofield N, Brown RJ, Holford SP (2016) The architecture of submarine monogenetic volcanoes - insights from 3D seismic data: Basin Res 30: 437–451. https://doi.org/10.1111/bre.12230

Robertson J, Ripley EM, Barnes SJ, Li C (2015) Sulfur liberation from country rocks and incorporation in mafic magmas: Econ Geol. https://doi.org/10.2113/econgeo.110.4.1111

Schofield N, Jerram DA, Holford S, Stuart A, Niall M, Hartley A, Howell J, David M, Green P, Hutton D, Stevenson C (2016) Sills in sedimentary basin and petroleum systems: In Németh K (ed) The Series Advances in Volcanology, pp 1–22.

Sewell RJ (1988) Late Miocene volcanic stratigraphy of central Banks Peninsula, Canterbury, New Zealand pp. 41–64. https://doi.org/10.1080/00288306.1988.10417809

Single RT, Jerram DA (2004) The 3-D facies architecture of flood basalt provinces and their internal heterogeneity: examples from the Palaeogene Skye Lava Field. J Geol Soc 161: 911-926

Smith KL, Milnes AR, Eggleton RA (1987) Weathering of basalt: formation of iddingsite. Clays Clay Miner 35: 418– 428

Schiøler P, Raine JI, Griffin A, Hollis CJ, Kulhanek DK, Morgans HEG, Roncaglia L, Strong CP, Uruski C (2011) Revised biostratigraphy and well correlation, Canterbury Basin, New Zealand. GNS Science Consultancy Report 2011/12. 142 p.

Stroncik NA, Schmincke HU (2002) Palagonite - A review: Int J Earth Sci. https://doi.org/10.1007/s00531-001-0238-7

Strogen DP, Seebeck H, Nicol A, King PR (2017) Two-phase Cretaceous–Paleocene rifting in the Taranaki Basin region, New Zealand; implications for Gondwana break-up: Journal of the Geological Society, https://doi.org/10.1144/jgs2016-160

Suggate RP, Stevens GR, Te Punga MT (1978) The geology of New Zealand. Govt Printer, Wellington.

Svensen HH, Planke S, Neumann ER, Aarnes I, Marsh JS, Polteau S, Harstad C, Chevallier L (2018) Sub-volcanic intrusions and the link to global climatic and environmental changes. In: Breitkreuz C., Rocchi S. (eds) Physical Geology of

Shallow Magmatic Systems. Advances in Volcanology. Springer. https://doi.org/10.1007/978-3-319-14084-1_10.

Svensen HH, Planke S, Malthe-Sørenssen A, Jamtveit B, Myklebust R, Eidem T, Rey S S (2004) Release of methane from a volcanic basin as a mechanism for initial Eocene global warming. Nature, 429, 542-545.

Timm C, Hoernle K, Werner R, Hauff F, van den Bogaard P, White J, Mortimer N, Garbe-Schönberg D (2010) Temporal and geochemical evolution of the Cenozoic intraplate volcanism of Zealandia. https://doi.org/10.1016/j.earscirev.2009.10.002

Walker F (1957) Ophitic Texture and Basaltic Crystallization. J Geol 65: 1-14. http://www.jstor.org/stable/30064199.

Walker GPL, Croasdale R (1971) Characteristics of some basaltic pyroclastics: Bull Volcanol. https://doi.org/10.1007/BF02596957

White JDL (2000) Subaqueous eruption-fed density currents and their deposits: Precambrian Res 101: 87–109. https://doi.org/10.1016/S0301-9268(99)00096-0

White JDL, Ross PS (2011) Maar-diatreme volcanoes: A review. https://doi.org/10.1016/j.jvolgeores.2011.01.010

White JDL, Valentine GA (2016) Magmatic versus phreatomagmatic fragmentation: Absence of evidence is not evidence of absence. Geosphere 12: 1478–1488. https://doi.org/10.1130/GES01337.1

Zimanowski B, Büttner R, Lorenz V, Häfele HG (1997) Fragmentation of basaltic melt in the course of explosive volcanism. J Geophys Res Sol Earth. doi:10.1029/96JB02935